frontiers | Frontiers in Materials

TYPE Original Research
PUBLISHED 11 April 2023
DOI 10.3389/fmats.2023.1134622

OPEN ACCESS

EDITED BY
Shengwen Tang,
Wuhan University, China

REVIEWED BY
Zhen Li,
Yangtze University, China
Wang Lei,
Xi'an University of Architecture and Technology, China

*CORRESPONDENCE
Fufei Wu,
201608014@gznu.edu.cn
Lilan Xie,
xielilan@gznu.edu.cn

SPECIALTY SECTION
This article was submitted to Structural Materials, a section of the journal Frontiers in Materials

RECEIVED 30 December 2022
ACCEPTED 21 March 2023
PUBLISHED 11 April 2023

CITATION
Dong S, Tu S, Chen L, Wu F, Xie L, Zhuo Q and Yu S (2023), Investigation of the performance of cement mortar incorporating lithium slag as a super-fine aggregate.
Front. Mater. 10:1134622.
doi: 10.3389/fmats.2023.1134622

Investigation of the performance of cement mortar incorporating lithium slag as a super-fine aggregate

Shuangkuai Dong[1], Shengwen Tu[1], Liangliang Chen[2,3], Fufei Wu[1]*, Lilan Xie[1]*, Qi Zhuo[1] and Songhan Yu[1]

[1]School of Materials and Architectural Engineering (Guizhou School of Emergency Management), Guizhou Normal University, Guiyang, China, [2]School of Civil Engineering, Huzhou Vocational and Technical College, Huzhou, China, [3]Huzhou Key Laboratory of Green Building Technology, Huzhou, China

As a by-product of lithium salt mining, the emission of lithium slag increases yearly due to increased demand. Therefore, the utilization of lithium slag faces a huge challenge. In this study, a new approach to using lithium slag as a super-fine aggregate in cement systems was proposed. The use of lithium slag as a super-fine aggregate replacing 0%, 30%, 50%, 70%, and 100% of the standard sand was tested. The main hydration products of cement–lithium slag paste were calcium silicate hydrate gel, calcium hydroxide, unhydrated particles, and a small amount of ettringite. Lithium slag as a super-fine aggregate could significantly reduce the dead load of structures, enhance flexural and compressive strength and the peak stress of mortar, and no more than 50% lithium slag could significantly enhance the permeability of mortar. The study revealed that the replacement rate of lithium slag as a super-fine aggregate could reach 50%, which is five times more than the amount used as supplementary cementitious material. Therefore, the study brings an innovation in the use of lithium slag in cement systems and improves the performance of cement mortar.

KEYWORDS

lithium slag, mortar, super-fine aggregate, mechanical property, water absorption

1 Introduction

Lithium slag is the by-product of lithium salt production, and 8–10 tons of lithium slag will be discharged by manufacturing 1 ton of lithium salt (Wang et al., 2020; Ali et al., 2021). The amount increases yearly due to the rapid development of China's lithium salt industry and the increased demand for lithium salt (Wu et al., 2018). It is reported that the global production of lithium salt is more than 1,200,000 tons annually, of which more than 800,000 tons are produced in China (Tan et al., 2020). However, less than 10% of lithium slag is utilized as a supplementary cementitious material for building material. Therefore, a large amount of lithium slag is landfilled, causing ecological environmental problems and wasting natural resources (Lu et al., 2023; Cui and Chang, 2022). Few studies have examined the technology of the use and recovery of lithium slag. Exploring uses of lithium slag is beneficial to the sustainable development of lithium salt industry, saves natural resources, and protects the environment (Li et al., 2021; Dong et al., 2023).

The demand for concrete in construction has caused a shortage of natural resources and deterioration of the environment which, in turn, have led to a need for innovation in

concrete technology. Global environmental concerns have been expressed by new legislation and commercial trends that require the concrete industry to minimize its environmental impact, mainly by reducing CO_2 emissions and natural resource consumption (Cui et al., 2022; Zhang et al., 2023). To deal with this problem, the concrete industry is aiming to produce concrete with environmental, economic, and technological benefits and innovations. In developed and developing countries, the utilization rate of waste has increased significantly, due to government support for the implementation of new technologies and standards, especially in the cement mortar and concrete industry (Huang et al., 2021; Peng et al., 2022). New products and technologies return economic income for the concrete industry and reduce the negative effect of waste materials on natural resources and the environment.

Concrete is the most used construction material, and there is a high potential to improve existing products and recycle waste material into new and useful products (Hlobil et al., 2022). Waste materials such as bottom ash, waste marble, waste crushed tile, and fly ash (Wang et al., 2022) have been evaluated for use as fine aggregate in cement mortar and concrete (Abebaw and Vadivu, 2021; Al-Lebban et al., 2021). For example, Singh and Siddique (2014) investigate the usability of bottom ash as a fine aggregate in cement-based concrete. The results show that there is no strength loss in the compressive strength of the concrete comparing to conventional concrete, although the usage of 100% bottom ash as natural sand in concrete. However, bottom ash uses as fine aggregate in concrete, which increases the water demand to obtain the same workability. Gencel et al. (2012) use waste marble as an aggregate and partially replace natural aggregate. The results of experimental study show that paving blocks manufactured with waste marble have enough compressive strength and increase wear resistance and freeze–thaw durability, so waste marble can be used as fine aggregate in paving block production. Topcu and Bilir (2010) manufacture cement mortar where natural aggregates are partly replaced by waste crushed tile. The results show a compressive strength above 20 MPa when the usage of crushed tile less than or equal to a ratio of 60%, and this ratio also reduces drying shrinkage and crack. Turhan et al. (2015) investigate the effect of fly ash as a fine aggregate in mortar. Flow ability, unit weight, ultrasound pulse velocity, compressive strength, flexural strength, modulus of elasticity, stress–strain behavior, free drying, and restrained shrinkage are discussed. The results show that the usage of fly ash as a fine aggregate presents a new approach to reusing a large amount of fly ash without causing significant changes in the properties of mortar when it is used at the ratio of 60%–70%. However, most studies ignore the experimental use of lithium slag as a super-fine aggregate.

Several papers have examined the use of lithium slag in cement and concrete technology (Luo et al., 2021; Li et al., 2019; Shi et al., 2020; Li and Yan, 2020), where it is considered a complementary cementitious material or partial replacement for cement at a replacement rate of up to 25%–40%. However, lithium slag has not been considered as a fine aggregate in mortar or concrete until now. Because fine aggregate in mortar occupies a high volume of about 60–75 wt.%, the performance and chemical composition of super-fine aggregates significantly influence the performance of mortar or concrete. In addition, the main chemical components of lithium slag are Al_2O_3, SiO_2, CaO, and Fe_2O_3, which is very similar to steel slag, phosphorus slag, and fly ash. Steel slag is a solid waste produced by steelmaking, containing a small amount of SO_2. Its main components are *f*-CaO, *f*-MgO, and FeO (Aparicio et al., 2020; Li et al., 2023). Its porous surface and chemical composition affect the workability, strength, and durability of concrete, especially the volume stability (Beaucour et al., 2020; Chen et al., 2021). However, steel slag also can replace some aggregates to reduce shrinkage deformation, and its specific volume expansion compensates for the internal shrinkage of concrete (He et al., 2021). Phosphorus slag is a by-product of the yellow phosphorus industry, and its vitreous content can generally reach 85–90 wt.%. It has potential gelling properties. Appropriate amounts of phosphorus slag can improve the microstructure and hydration performance of concrete at an early stage (Yong et al., 2022). The porosity and accumulated pore volume of concrete containing phosphorus slag decrease with the prolongation of curing time. In addition, the finer the phosphorus slag particles, the more uniform the medium distribution, which can improve the compressive strength of concrete (Yang et al., 2021; Mehdizadeh et al., 2022). Fly ash is a fine powder produced during fuel combustion. Adding a proper amount of fly ash can improve the total pore area, average pore size and total porosity of concrete and improve its mechanical properties (Javed et al., 2022). At the same time, the addition of fly ash can reduce the hydration heat, reduce the probability of early thermal cracking, and reduce the autogenous volume deformation the initial strength of concrete (Wang et al., 2020; Grabias-Blicharz and Franus, 2023). However, lithium slag, unlike steel slag, phosphorus slag, and fly ash, is not easy to obtain, and it is produced in relatively few areas. Even in China, it is only distributed in Mianyang, Sichuan, and Urumqi, Xinjiang. Therefore, the research on lithium slag as a super-fine aggregate has not received enough attention.

In this study, the evaluation of lithium slag as a super-fine aggregate in mortar is investigated. Some properties of mortar are discussed, such as hydration products, $Ca(OH)_2$ content, Fourier spectrum, unit weight, compressive strength, flexural strength, stress–strain, and water absorption rate. The work provides guidance about utilizing lithium slag as a super-fine aggregate extensively and efficiently, so that it can be better applied in engineering and construction to ameliorate ecological and environmental problems. The experimental materials and the associated experimental program and testing procedure are described in detail in Section 2. The results of the study are analyzed and discussed in Section 3, and finally, Section 4 concludes.

2 Materials and methods

2.1 Experimental materials

The P.O42.5R Ordinary Portland cement came from China's XiNan cement factory. Its specific surface area was 387 m^2/kg, the density was 3.15 g/cm^3, and the compressive strength was 18.7 MPa at 3 days, 29.8 MPa at 7 days, and 44.5 MPa at 28 days according to the Chinese standard GB175-2007. The chemical composition of cement is displayed in Table 1. A superplasticizer from Laiyang Hongyang construction admixture factory of China was employed to provide a satisfactory workability. Standard sand with a high silica

TABLE 1 Chemical composition of cement and lithium slag.

Name	SiO_2	Al_2O_3	Fe_2O_3	CaO	MgO	SO_3	Na_2O	K_2O
Cement/wt.%	28.1	6.38	4.29	54.87	2.69	2.67	0.36	0.64
Lithium slag/wt.%	6.9	55.65	21.63	6.43	2.59	2.95	2.72	1.13

TABLE 2 Mix of cement–lithium slag mortar.

No.	Cement/g	Water/g	Standard sand/g	Lithium slag/g	High-rate superplasticizer/g
C	450	225	1350	0	0
L1	450	225	945	405	8.55
L2	450	225	675	675	11.25
L3	450	225	405	945	13.95
L4	450	225	0	1350	18.00

content was used as the reference sand to produce cement mortar; its particle size was kept below 2.35 mm, and it was made by China's Xia Men ISO Standard Sand Co., Ltd.

Lithium slag (LS) used as a super-fine aggregate to replace standard sand came from China's Xinjiang lithium salt factory. The specific surface area was 400 m^2/kg, and its chemical composition is displayed in Table 1. By comparison, the standard sand is coarser than the lithium slag, which may lead to an increment in water demand (Shi et al., 2020). However, the usage of superplasticizers decreased the need for water. In this study, the standard sand was replaced by an equal weight of lithium slag.

2.2 Experimental methods

The water–cement ratio was 0.50, the mass ratio of cement and standard sand was 1:3, and the mass ratio of cement:water:standard sand was 450:225:1350. Specimens (40 mm × 40 mm × 160 mm) of each proportional mixture were prepared with standard sand, superplasticizer, Portland cement, water, and lithium slag as a super-fine aggregate, respectively. According to the studies of Shi et al. (2020) and Li et al. (2019), when lithium slag replaced 30% of cement, its performance was basically equivalent to that of pure cement cementitious material because lithium slag could play a micro-aggregate effect. Therefore, 0%, 30%, 50%, 70%, and 100% proportions of lithium slag were considered super-fine aggregates instead of standard sand. The cement paste/mortar was identified as C, and the cement–lithium slag paste/mortar samples with 30%, 50%, 70%, and 100% lithium slag were marked as L1, L2, L3, and L4, respectively. The mix ratios of cement–lithium slag mortar and sample numbers are shown in Table 2. A flow table test was performed on fresh mortar to determine the effect of the lithium slag on workability. Specimens were molded when the flow table test was the same, placed at 20 °C and 95% relative humidity for 24 h and then demolded, and cured at 20 °C ± 1 °C and 95% relative humidity for 7 and 28 days. Then, their hydration product, $Ca(OH)_2$ content, Fourier spectrum, compressive strength, flexural strength, unit weight, absorption water rate, and stress–strain were investigated.

Cement paste and cement–lithium slag paste (without standard sand) were molded in 10 mL of the centrifugal tube, the cap was tightened, and the samples were sent to the curing room (20 °C ± 1 °C, 95% or higher humidity). After curing for 7 and 28 days, the tube was broken, and the sample was soaked in anhydrous ethanol for 24 h to discontinue hydration and Guaranteed crushing fineness of grinding (sieving 0.1 mm). XRD and thermogravimetric experiments were carried out by SMART APEX Ⅱ-type X-ray polycrystalline crystal diffraction produced by German Brooke AXS Co., Ltd. and a STA449F3-type synchronous thermal analyzer produced by the German Resistance Company, respectively. The finely ground paste was mixed with the dried and grained KBr at a 1:200 ratio, and the Fourier spectrum and the film were tested by WQF-520 type Fourier transform infrared spectroscopy.

Unit weight was tested by the weighing method. The flexural strength and compressive strength were tested using an EPC70-type automatic bending device and a YAW-300B-type computer control electro-hydraulic cement pressure testing machine produced by the Hangzhou Xin High Tech Co. Ltd. according to the "cement mortar strength test method (GB/T 17671-2021)." Stress–strain was tested according to the "Standard for test methods of concrete physical and mechanical properties (GB/T 50081-2019)." Water absorption was tested according to the "Test methods for bulk density, moisture, and water absorption of aerated concrete (GB/T 11969-2008)."

3 Results and discussion

3.1 Hydration product

Usually, the main products after cement hydration are calcium silicate hydrate, calcium ferrite hydrate, portlandite, calcium aluminate hydrate, calcium sulphoaluminate hydrate, ettringite, and cement clinker particles that have not been hydrated (Shi et al., 2020). The influence of lithium slag on cement hydration products is shown in Figure 1.

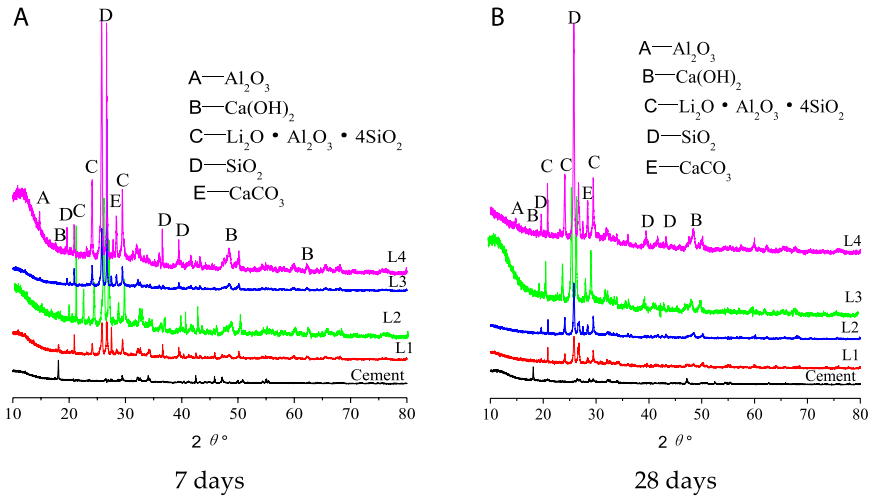

FIGURE 1
XRD spectrum of cement paste and cement–lithium slag paste.

L1 in Figure 1A shows that after adding 30% lithium slag, the main crystalline hydration products were calcium silicate hydrate, portlandite, unhydrated particles, and a trace of $CaCO_3$ and Li_2CO_3. Unhydrated particles mainly contained Al_2O_3, SiO_2, and $Li_2O{\cdot}Al_2O_3{\cdot}SiO_2$, and the $CaCO_3$ due to portlandite was carbonated in the process of grinding. With the increase of lithium slag replacement, the main diffraction peak of unhydrated particles became more acute, which had a low content of portlandite in cement early hydration (such as the curves of Figure 1A). Besides, the activity of lithium slag was relatively lower and the replacement was larger (Wu et al., 2016a; Wu et al., 2016b), so the diffraction peaks of unhydrated particles were acute keen (such as the curves of L4 in Figure 1A), which could be explained by the fact that Al_2O_3 and SiO_2 had not sufficiently participated in the secondary hydration. In addition, it was proposed that ettringite (AFt) was not identified due to the slightly low diffraction peak. Meanwhile, with the increase of curing age from 7 days to 28 days, the diffraction peaks of Al_2O_3, SiO_2, $Li_2O{\cdot}Al_2O_3{\cdot}SiO_2$, and portlandite became significantly lower. Especially in the curves of L2 and L3 in Figure 1B, the diffraction peaks of unhydrated particles and portlandite became significantly lower than the equivalent peaks of L2 and L3 in Figure 1A, indicating that Al_2O_3 and SiO_2 had participated in the secondary hydration, resulting in a significant decrease in portlandite at 18.2° and a significant increase in portlandite at 47.2°. However, after 100% lithium slag replaced the fine aggregate, the diffraction peaks of unhydrated particles were still the most prominent, which once again showed that the activity of lithium slag was low (Shi et al., 2020). Therefore, the diffraction peaks of calcium ferrite hydrate, calcium hydroxide, calcium aluminate hydrate, and calcium sulphoaluminate hydrate were still insignificant.

3.2 $Ca(OH)_2$ content

The hydration product of cement–lithium slag paste can be analyzed qualitatively and quantitatively for calcium silicate hydrate gel, portlandite, and ettringite by thermogravimetric analysis (TG) (Liu et al., 2015; Hu et al., 2021). Figure 2 and Figure 3 show the TG curves of hydration products for pure cement paste and cement–lithium slag paste with 30%–100% lithium slag at 7 days and 28 days. From Figure 2 and Figure 3, it can be seen that the TG curve was divided into four stages, which was similar between pure cement paste and cement-lithium slag paste in 20°C~900°C. The first stage is the ettringite dehydration stage at 50 °C–200 °C, the second stage is the portlandite dehydration stage at 400 °C–550 °C, the third stage is the calcium carbonate dehydration stage at 550 °C–770 °C, and the fourth stage is the $CaCO_3$ and Li_2CO_3 dehydration stage at 800 °C–900 °C (Li and Yan, 2010; Chen et al., 2011). Therefore, the content of CH can be calculated according to the dehydration stage at 400 °C–550 °C. The results are shown in Figure 4.

The CH content of pure cement paste was 5.63% at 7 days and 6.12% at 28 days. The CH content of cement–lithium slag paste after adding 30%–100% lithium slag as a super-fine aggregate is shown in Figure 4. It can be seen from Figure 4 that the CH content of the cement–lithium slag paste significantly decreased with the increasing amount of lithium slag. The equations are $CH = -0.0148x + 3.933$ at 7 days and $CH = -0.0152x + 4.007$ at 28 days, and the correlation coefficients are $R^2 = 0.8663$ and $R^2 = 0.8864$ at 7 days and 28 days, respectively. We can estimate the content of CH under different replacement amounts of lithium slag using these linear formulas. In addition, the change in the CH content of cement–lithium slag paste with the same replacement ratio at 7 days and 28 days was small, at about 65.0% and 60.6% of pure cement paste, respectively. It can be explained that the activity of lithium slag was also relatively lower, but it could still participate in partial secondary hydration reaction; mainly, Al_2O_3 and SiO_2 in lithium slag reacted with CH to generate calcium aluminate hydrate and calcium silicate hydrate. Therefore, adding 30%–100% lithium slag as a super-fine aggregate in a cement system, which increased the amount of hydrated calcium silicate and hydrated calcium aluminate, also improved the mechanical properties and durability of cement mortar, as will be discussed in the following sections.

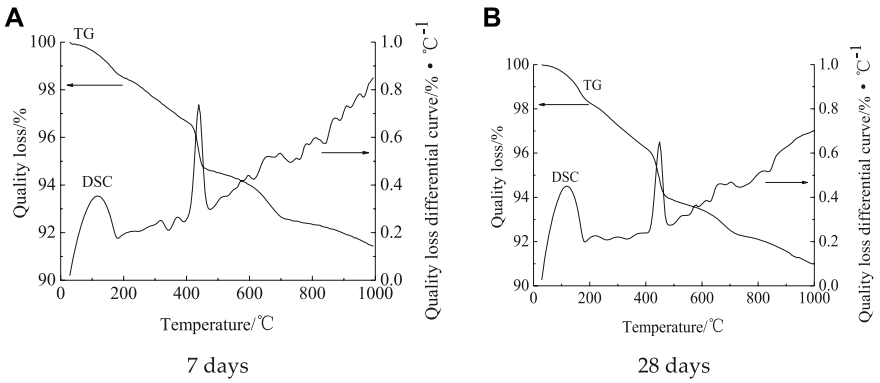

FIGURE 2
TG curve of pure cement paste.

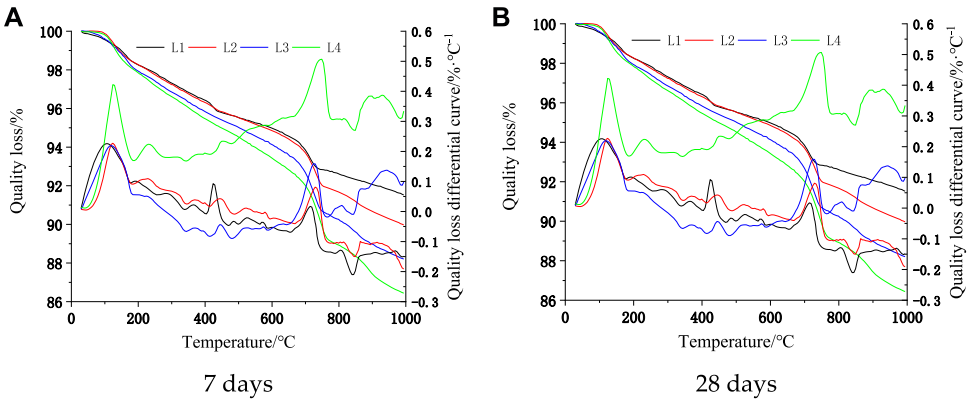

FIGURE 3
TG curve of cement paste with lithium slag.

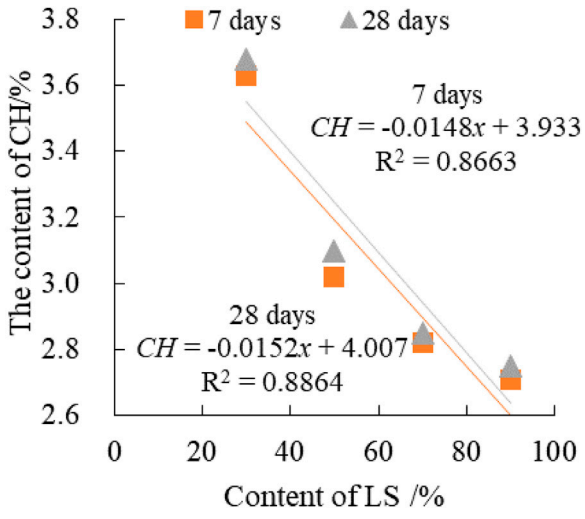

FIGURE 4
$Ca(OH)_2$ content.

3.3 Fourier spectrum

Figure 5 shows the spectral characteristic of cement–lithium slag paste under different replacement amounts. It can be seen from Figure 5 that the characteristic peaks of cement–lithium slag paste were mainly 3467 cm^{-1}, 3438 cm^{-1}, 2923 cm^{-1}, 2348 cm^{-1}, 1638 cm^{-1}, 1429 cm^{-1}, 1111 cm^{-1}, 1000 cm^{-1}, 768 cm^{-1}, 696 cm^{-1}, and 462 cm^{-1} at 7 days and 28 days, respectively. With increasing lithium slag replacement, the characteristic 7-day peak in 3467 cm^{-1} became smaller and even disappeared when the replacement rate reached 100%. This behavior is the reverse of the behavior of the characteristic peak in 3438 cm^{-1}; namely, its intensity peaked when the replacement rate reached 100%, revealing that with increasing lithium slag replacement, the content of hydration product CSH increased, but the content of CH decreased. This illustrates that lithium slag can participate in the secondary hydration reaction; it consumes CH and forms a certain amount of CSH. The characteristic peak in 2923 cm^{-1} increased with the increase of lithium slag replacement; it was the largest when the replacement rate reached 100%. This illustrates

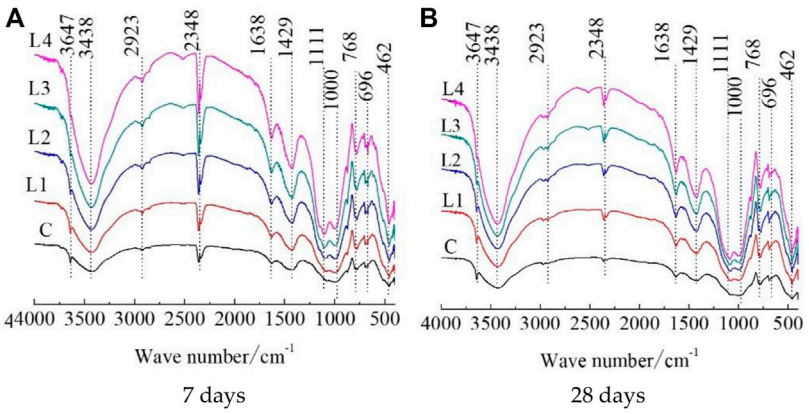

FIGURE 5
Spectral characteristics of cement–lithium slag paste.

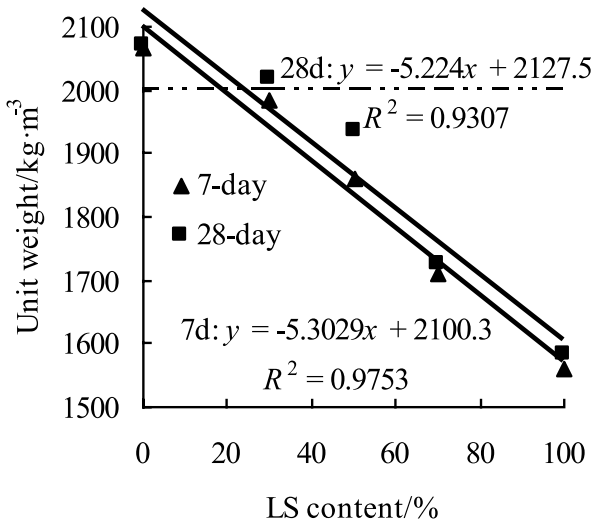

FIGURE 6
Unit weight.

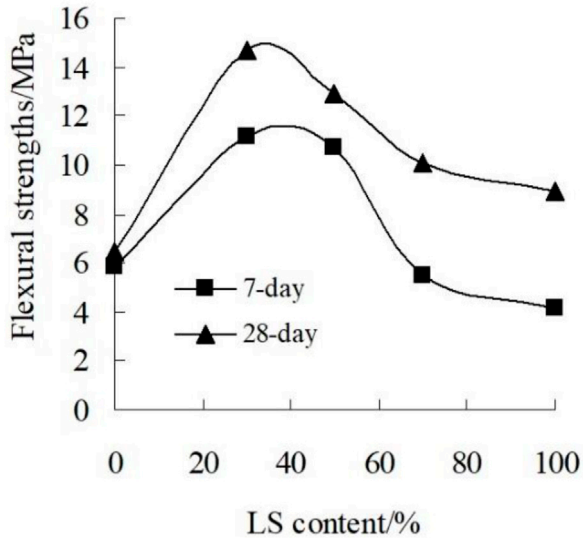

FIGURE 7
Flexural strength.

that the O–H content increases, which is mainly composed of CSH gel in the paste and free water adsorption of lithium slag; therefore, the O–H content is considerably larger when the lithium slag replacement rate is 100%. The change law of wave number 2348 cm^{-1} was similar to that at 2923 cm^{-1}, but the peak intensity at 28 days was bigger than that of the others at 7 days. The size of this peak is mainly caused by Li_2CO_3 in lithium slag and carbonized CH in paste, which leads to the peak intensity being larger at 2348 cm^{-1}. The change law of wave numbers 1638 cm^{-1} and 2348 cm^{-1} was similar to that of 2348 cm^{-1} and 2923 cm^{-1}, and the variation was also small as the curing age increased from 7 days to 28 days. The change is mainly caused by $CaSO_2{\cdot}2H_2O$ and AFt in paste, which can effectively improve the properties of the paste. Simultaneously, the change law of wave numbers 696 cm^{-1} and 462 cm^{-1} at 7 days and 28 days was similar to that of 2348 cm^{-1}, 2923 cm^{-1}, and 1638 cm^{-1} with increasing lithium slag replacement.

3.4 Unit weight

The unit weight of cement mortar with lithium slag as a superfine aggregate is presented in Figure 6.

From Figure 6, it can be seen that the unit weight of cement mortar with lithium slag at the age of 7 days and 28 days showed a downward trend with increasing amounts of replacement, and the change of their peak unit weight depended on the content of lithium slag.

As a control group, the unit weight of cement mortar was 2065.04 kg/m^3 at 7 days and 2017.68 kg/m^3 at 28 days. After

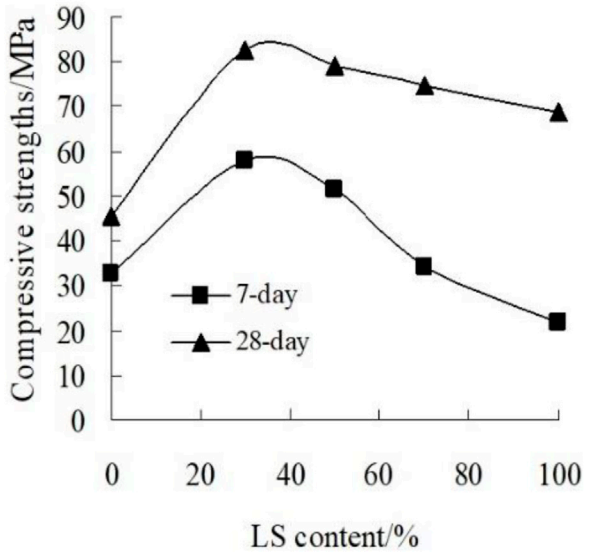

FIGURE 8
Compressive strength.

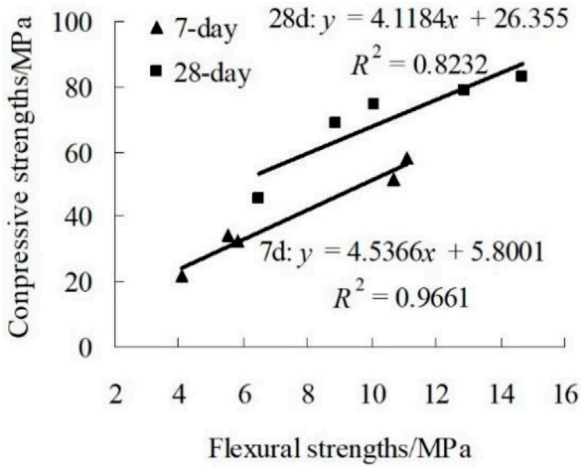

FIGURE 9
Correlation of compressive and flexural strength.

adding 30%, 50%, 70%, and 100% lithium slag as a super-fine aggregate, 7-day unit weights varied between 1983.91 and 1560.12 kg/m^3, while 28-day weights changed between 2017.34 and 1582.54 kg/m^3, a decrease of 3.95%–24.45% at 7 days, and 2.62%–23.61% at 28 days, compared with the control group. Therefore, as expected, adding lithium slag as a super-fine aggregate resulted in lower unit weight at 7 and 28 days than pure cement mortar. This reason is that the specific gravity of lithium slag is 2.48 g/cm^3, which is less than that of standard sand. Thus, the more lithium slag is added, the smaller the unit weight of mortar is. (Snellings et al. (2022) classify as lightweight, half-structural, and isolation concrete according to their unit weights, which are 0–2000, 2000–2,800, and above 2,800 kg/m^3, respectively. Lightweight concrete was achieved in this study when the replacement amount was 50%, 70%, and 100%. This reduction significantly reduced the dead load of the concrete structure (Xian and Shao, 2021). In addition, the relationship between the unit weight of mortar and lithium slag content is also presented in Figure 6. There is a high linear correlation between the unit weight of mortar and lithium slag content, at R^2 = 0.9753 at 7 days and R^2 = 0.9307 at 28 days. Therefore, $y = -5.3029x + 2100.3$ and $y = -5.224x + 2127.5$ could be used to predict the unit weight of mortar with lithium slag at 7 days and 28 days, respectively. As clearly shown from these findings, a high content of lithium slag will result in reduced unit weight.

3.5 Flexural strength

Although the compressive strengths of cement mortar and concrete are considered in concrete structural design, their flexural strengths are also important in applications such as dams and highways (Youm et al., 2014). The flexural strength change of cement mortar with lithium slag as a super-fine aggregate is presented in Figure 7. It can be seen from Figure 7 that the flexural strength development of cement mortar presented an increasing trend and then decreased with the increment of lithium slag content. The change of the peak flexural strength depended on the content of lithium slag.

As a control group, the flexural strength of cement mortar was 5.82 MPa at 7 days and 6.46 MPa at 28 days. The peak flexural strength value that appeared in the replacement amount was 30%, which was 11.11 MPa at 7 days and 14.70 MPa at 28 days, an increase of 90.89% and 127.55% compared with the control group. As the replacement amount increased, the flexural strength of the mortar decreased. For example, when the replacement amount of lithium slag was 100%, the flexural strength decreased by 29.21% at 7 days and increased by 37.77% at 28 days compared with the control group. Longer curing time can result in increasing flexural strength. On the one hand, it is clear from Figure 7 that the volcanic ash activity of the lithium slag had an important influence on flexural strength, which led to an increase of 90.89% at 7 days and 127.55% at 28 days. On the other hand, adding 30%, 50%, 70%, and 100% lithium slag as a super-fine aggregate could improve the interfacial transition zone of mortar. In addition, the hydration rate of cement decreased as the amount of lithium slag increased. The flexural strength of mortar with lithium slag as a super-fine aggregate decreased with a higher replacement ratio.

3.6 Compressive strength

Compressive strength, a vital element of concrete structural design, is the most important property of cement mortar and concrete. Compressive strength results of cement mortar with lithium slag as a super-fine aggregate are presented in Figure 8. From Figure 8, it can be seen that the compressive strength of cement mortar with lithium slag at the age of 7 days and 28 days showed a downward trend after rising first, and the change of the peak compressive strength depended on the content of lithium slag.

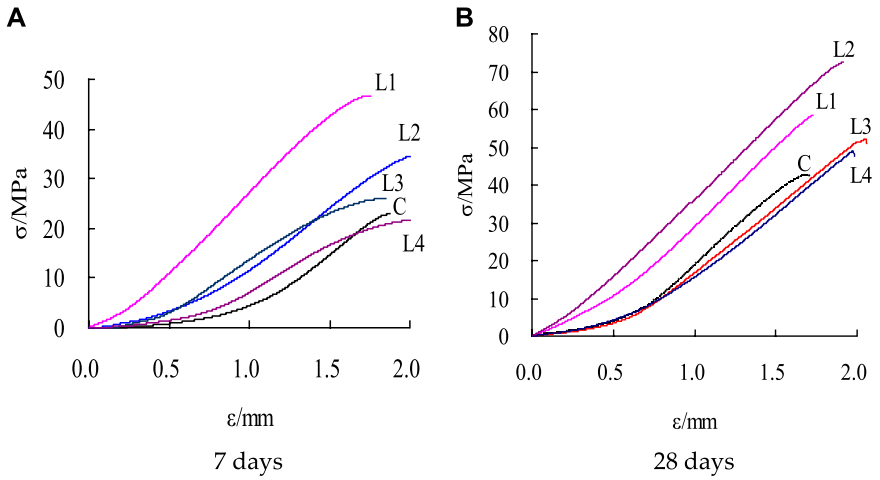

FIGURE 10
Stress–strain curve of mortar.

The compressive strength of the control group cement mortar was 32.4 MPa at 7 days and 45.3 MPa at 28 days. After adding 30%–100% lithium slag as a super-fine aggregate, the compressive strength varied between 57.91 MPa and 21.70 MPa at 7 days and between 82.72 MPa and 68.81 MPa at 28 days, a decrease of 78.70% ~−33.02% at 7 days and 82.56–51.89% at 28 days, compared with the control group. Like the trend of flexural strength with content, the peak value of compressive strength appeared in the 30% replacement amount, where it was an increase of 78.70% at 7 days and 82.56% at 28 days compared with the control group. The compressive strength decreased by 33.02% for 7 days, while it increased by 51.88% for 28 days when the replacement rate of lithium slag was 100%. As clearly shown here, the compressive strength of mortar with 100% lithium slag is higher than that of pure cement mortar. The reason is that lithium slag is finer than cement and better fills gel pores, improving the compactness of mortar. The hydration of cement can be increased by adding lithium slag, and cementitious hydrated calcium silicate can be formed. In addition, the connection of cement particle hydration product was dispersed due to the lower activity of lithium slag; the higher the replacement rate was, the more significant the dispersion effect. The thermo-gravimetric and infrared spectra results also showed the same finding; the higher the content of non-binding substances such as lithium slag and lithium carbonate was, the more limited the formation of hydrated calcium silicate was, which affected the mechanical properties of the mortar. Overall, the mechanical property of mortar reached the highest value when the lithium slag content was 30%. The relationship between compressive strength and flexural strength is presented in Figure 9. There was a high linear correlation between compressive strength and flexural strength, with R^2 = 0.9661 at 7 days and R^2 = 0.8232 at 28 days. Compressive strength is directly related to flexural strength. The strength of mortar with 100% lithium slag as a super-fine aggregate instead of standard sand was higher than that of pure cement mortar, which means a higher usage ratio of lithium slag as a super-fine aggregate instead of standard sand is possible for the production of lightweight concrete.

3.7 Stress–strain

The stress–strain curve, a relationship model for concrete structure non-linear analysis and ultimate bearing capacity analysis, is an important basis for studying the bearing capacity and deformation of a concrete structure (Guo et al., 2022). Figure 10 shows the stress–strain curve of mortar at different replacement percentages and curing ages. It changed at different replacements and curing ages, following a consistent pattern. After adding 30%, 50%, 70%, and 100% lithium slag as a super-fine aggregate, the peak stress of mortar at 7 days was 2.04, 1.52, 1.14, and 0.95 times that of the control group, while the peak stresses of mortar at 28 days were 1.39, 1.73, 1.23, and 1.21 times that of the control group. Therefore, it was feasible to prepare lightweight concrete using lithium slag instead of standard sand, which could increase the use of solid waste in mortar and concrete. The displacement of mortar with lithium slag was larger than that of cement mortar at 7 days and 28 days. All were within 0.2 mm at 7 days, while the displacement could reach 0.4 mm at 28 days. Based on the literature method of calculating external load work (Jian et al., 2016), it was found that the external load work of mortar decreased from 66.91 MPa to 37.78 MPa when the replacement percentage of lithium slag increased from 30% to 100%. However, the external workload of mortar with increasing percentages of lithium slag was nevertheless 2.99, 2.60, 1.84, and 1.69 times higher than that of pure cement mortar at 7 days, while it was 1.68, 2.44, 1.42, and 1.33 times higher than pure cement mortar at 28 days.

The relationship between external load work and the replacement rate of lithium slag was established to analyze the mechanical properties of mortar. The results are shown in Figure 11, which shows that the peak stress ratio of mortar at 7 days and 28 days decreased linearly as the replacement increased from 30% to 100%. The relationships were R^2 = 0.9543 at 7 days and R^2 = 0.5639 at 28 days, respectively. The change laws of external load work were similar to peak stress; their relationships are R^2 = 0.9465 at 7 days and R^2 = 0.5439 at 28 days. It is also difficult to find that the mechanical property of mortar was better than that of

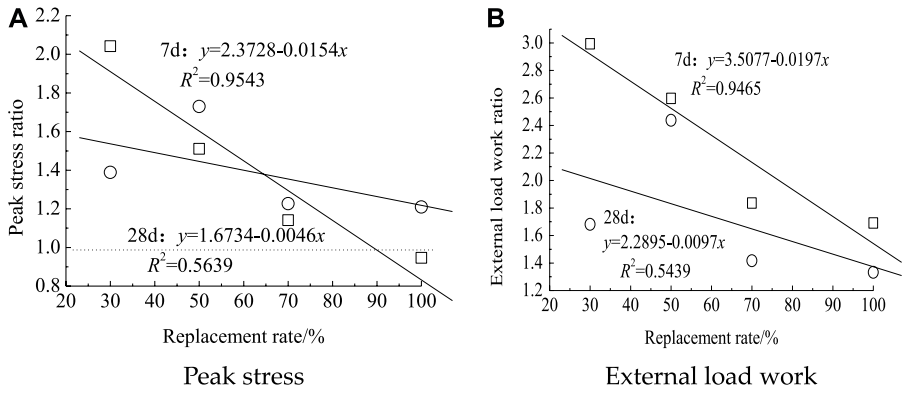

FIGURE 11
Peak stress and external load work of mortar at 7 days and 28 days.

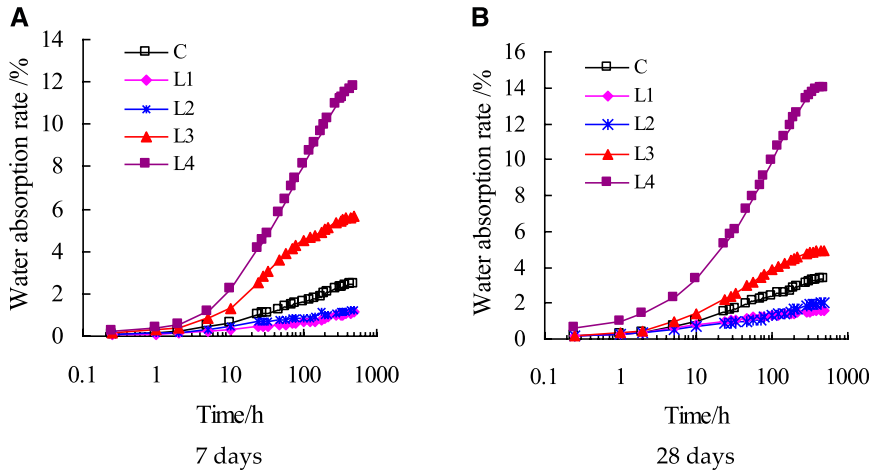

FIGURE 12
Water absorption rate of cement–lithium slag mortar.

pure cement mortar, except that the replacement rate was 100% at 7 days. In addition, the external load work ratio of mortar with 30%–100% lithium slag was above 1.0 at 7 days and 28 days, which further illustrated the advantage of mortar with lithium slag over that of pure cement mortar.

3.8 Water absorption

The water absorption rate is one way to measure cement mortar and cement concrete permeability, which is an important parameter to evaluate the durability of mortar and concrete. After adding 30%–100% lithium slag, the water absorption rate of mortar at 7 days and 28 days is shown in Figure 12, Table 3 and Table 4.

Figure 12A and Table 3 show that the water absorption rate of mortar increased as the percentage of lithium slag increased and reached a maximum at 483 h; after this, its change was less than that of pure cement mortar. When 100% lithium slag was added as a super-fine aggregate, the water absorption rate of mortar was 3.55 times that of pure cement mortar within 2 h. However, the change was within 12.6%, except when the replacement of lithium slag was 100%. The water absorption rate change of mortar with 0%–100% lithium slag was fast, which was from 1.37%, 0.39%, 0.39%, 0.36%, and 0.43% to 12.30%, 3.24%, 1.47%, 1.71%, and 4.93% within 2 h–216 h, while it was very slow after 216 h. Particularly, after 390 h, the water absorption rate fell by 0.5% every 50 h. The water absorption time was prolonged to 480 h, and the water absorption rate of the mortar increased gradually. It was 48.51%, 60.00%, 148.09%, and 416.89% that of pure cement mortar. A similar pattern is shown in Figure 12B and Table 4. Therefore, the water absorption rate was lower with lithium slag replacement and was less than 50% than that of pure cement mortar.

Based on the aforementioned experimental study, the replacement rate of lithium slag as a super-fine aggregate is

TABLE 3 Water absorption rate of cement–lithium slag mortar at 7 days.

Time/h	0.25	1	2	5	10	24	29	33	47	57	70	80
C/%	0.15	0.24	0.39	0.67	0.96	1.50	1.62	1.69	1.94	2.08	2.21	2.29
L1/%	0.17	0.27	0.39	0.60	0.77	1.00	1.05	1.07	1.16	1.20	1.24	1.26
L2/%	0.22	0.28	0.36	0.53	0.68	0.86	0.90	0.92	1.01	1.05	1.08	1.19
L3/%	0.19	0.36	0.43	0.94	1.39	2.21	2.41	2.53	2.95	3.19	3.44	3.60
L4/%	0.63	0.97	1.37	2.32	3.38	5.32	5.80	6.09	7.18	7.89	8.53	9.07
Time/h	100	124	144	175	194	216	284	321	343	390	439	483
C/%	2.41	2.51	2.58	2.64	2.79	3.24	3.82	3.98	4.02	4.11	4.16	4.19
L1/%	1.31	1.34	1.37	1.41	1.45	1.47	1.52	1.53	1.55	1.57	1.60	1.62
L2/%	1.29	1.37	1.42	1.48	1.63	1.71	1.85	1.89	1.93	1.95	1.99	2.01
L3/%	3.85	4.08	4.24	4.39	4.49	4.59	4.77	4.83	4.85	4.91	4.94	4.96
L4/%	9.96	10.74	11.29	11.87	12.30	12.59	13.36	13.58	13.69	13.85	13.94	13.96

TABLE 4 Water absorption rate of cement–lithium slag mortar at 28 days.

Time/h	0.25	1	2	5	10	24	29	33	47	57	70	80
C/%	0.07	0.14	0.22	0.42	0.62	0.97	1.05	1.10	1.26	1.34	1.46	1.51
L1/%	0.05	0.09	0.14	0.24	0.32	0.45	0.46	0.49	0.54	0.56	0.59	0.61
L2/%	0.07	0.12	0.18	0.30	0.50	0.66	0.69	0.72	0.76	0.79	0.81	0.82
L3/%	0.16	0.28	0.41	0.81	1.33	2.55	2.85	3.03	3.62	3.91	4.15	4.29
L4/%	0.20	0.35	0.55	1.12	2.18	4.11	4.52	4.82	5.79	6.44	7.07	7.44
Time/h	100	124	144	175	194	216	284	321	343	390	439	483
C/%	1.60	1.70	1.77	1.87	1.96	2.03	2.20	2.28	2.31	2.36	2.42	2.48
L1/%	0.66	0.68	0.72	0.75	0.84	0.91	0.98	1.01	1.02	1.06	1.08	1.12
L2/%	0.84	0.87	0.89	1.13	0.98	1.03	1.09	1.12	1.14	1.17	1.19	1.26
L3/%	4.49	4.66	4.76	4.88	5.02	5.16	5.39	5.47	5.52	5.57	5.61	5.66
L4/%	8.08	8.68	9.13	9.67	9.96	10.25	10.91	11.13	11.27	11.49	11.65	11.78

recommended to be not more than 50%, which is 675 g in this experiment. When using lithium slag as an admixture instead of cement, the content should not be more than 30%; in this test, that amount is 135 g (Shi et al., 2020). Therefore, five times as much lithium slag can be used as a super-fine aggregate than as an admixture instead of cement, and using lithium slag can not only greatly affect energy conservation and emission reduction but also improve the performance of mortar and concrete.

4 Conclusion

In this work, the effects of lithium slag as a super-fine aggregate on hydration products, $Ca(OH)_2$ content, Fourier spectrum, unit weight, compressive strength, flexural strength, stress–strain, and water absorption rate of cement mortar were studied. The main experimental results can be drawn as follows:

(1) The main crystalline hydration products were CSH gels, CH, unhydrated particles, and AFt when lithium slag was used as a super-fine aggregate. The CH content of cement–lithium slag paste was significantly reduced, while the content of $CaCO_3$ and Li_2CO_3 was significantly increased with increasing proportions of replacement.

(2) The unit weight of cement–lithium slag mortar was less than 2000 kg/m^3 over a range of 30% to 100% replacement rate, which significantly reduced the dead load of the concrete structure.

(3) The flexural strength and compressive strength of mortar vary between 14.7 MPa–9.8 MPa and 82.7 MPa–68.8 MPa, respectively, which are higher than those of pure cement mortar.

(4) The peak stress of cement–lithium slag mortar (30%, 50%,70%, and 100%) was 2.04,1.52, 1.14, and 0.95 times larger than that of pure cement mortar at 7 days, while it was 1.39, 1.73, 1.23, and 1.21 times larger at 28 days as the proportion of replacement

increased from 30% to 100%. The change law of external load work was similar to the peak stress, but it was above 1.0 under different replacement percentages.

(5) The water absorption rate of mortar increased as the amount of lithium slag increased, and it was lower at 7 days and 28 days than that of pure cement mortar when the replacement was less than 50%.

(6) The replacement rate of lithium slag as a super-fine aggregate was recommended to be not more than 50%, which was five times more than can be used when lithium slag was used as an admixture instead of cement.

The experimental investigation carried out in this work found that the examined cement–lithium slag mortar had adequate mechanical properties and durability for concrete structural usage, with remarkable unit weight and permeability. The replacement rate of lithium slag as a super-fine aggregate was 50%, which is a sustainable proposal for cement–lithium slag mortar production and use, as this use contributes to economizing fine aggregate when satisfying structural performance. Therefore, the extensive use of lithium slag meets the need for the sustainable development of the lithium salt industry and also improves the carbon reduction efforts of the cement industry, playing a positive role in realizing the Chinese double-carbon strategic task.

Data availability statement

The original contributions presented in the study are included in the article/Supplementary Material; further inquiries can be directed to the corresponding author.

Author contributions

Conceptualization, SD and FW; methodology, QZ; software, SY; validation, QZ, LX, and LC; formal analysis, SY; investigation, LX; resources, LX; data curation, FW; writing—original draft preparation, review, and editing, SD; visualization, FW and LL; supervision, QZ; project administration, FW; funding acquisition, FW and LC. All authors have read and agreed to the published version of the manuscript.

Funding

This study is supported by Guizhou Provincial Science and Technology Foundation (Qianke Joint Foundation ZK[2023] General 264, Qianke Joint Foundation ZK[2023] General 265 and Qianke Joint Foundation ZK[2021] General 294). The authors are extremely grateful to the support of school of materials and architectural engineering, Guizhou normal university.

Acknowledgments

The authors appreciate the aid provided by the reviewers and editors to improve the paper.

Conflict of interest

The authors declare that the research was conducted in the absence of any commercial or financial relationships that could be construed as a potential conflict of interest.

Publisher's note

References

Abebaw, L., and Vadivu, P. (2020). Combined effect of ambo stone as coarse aggregate and fly ash as cement on mechanical properties of concrete. *J. Eng. Appl. Sci.* 15 (15), 2977–2989. doi:10.13140/RG.2.2.36272.07685

Al-Lebban, M. F., Alhabbobi, A. M., Talib, A. G., and Jabal, Q. A. (2021). Influence of waste glass powder and crushed cobblestone on mechanical properties of concrete. *Phys. Conf. Ser.* 11, 012170. doi:10.1088/1742-6596/1973/1/012170

Ali, S. F., Chen, B., Ahmad, M. R., and Haque, M. A. (2021). Development of cleaner one part geopolymer from lithium slag. *J. Clean. Prod.* 291, 125241. doi:10.1016/j.jclepro.2020.125241

Alterary, S. S., and Marei, N. H. (2021). Fly ash properties, characterization, and applications: A review. *J. King Saud University-Science* 33 (6), 101536. doi:10.1016/j.jksus.2021.101536

Aparicio, S., Hernández, M. G., and Anaya, J. J. (2020). Influence of environmental conditions on concrete manufactured with recycled and steel slag aggregates at early ages and long term. *Constr. Build. Mater.* 249, 118739. doi:10.1016/j.conbuildmat.2020.118739

Beaucour, A. L., Pliya, P., Faleschini, F., Njinwoua, R., Pellegrino, C., and Noumowé, A. (2020). Influence of elevated temperature on properties of radiation shielding concrete with electric arc furnace slag as coarse aggregate. *Constr. Build. Mater.* 256 (13), 119385. doi:10.1016/j.conbuildmat.2020.119385

Chen, X., Fang, K. H., Yang, H. Q., and Peng, H. (2011). Hydration kinetics of phosphorus slag-cement paste. *J. Wuhan Univ. Technology-Materials Sci. Ed.* 26, 142–146. doi:10.1007/s11595-011-0186-4

Chen, Z. M., Li, R., Zheng, X. M., and Liu, J. X. (2021). Carbon sequestration of steel slag and carbonation for activating RO phase. *Cem. Concr. Res.* 139 (14), 106271. doi:10.1016/j.cemconres.2020.106271

Cui, K., and Chang, J. (2022). Hydration, reinforcing mechanism, and macro performance of multi-layer graphene-modified cement composites. *J. Build. Eng.* 57, 104880. doi:10.1016/j.jobe.2022.104880

Cui, K., Liang, K. K., Chang, J., and Lau, D. (2022). Investigation of the macro performance, mechanism, and durability of multiscale steel fiber reinforced low-carbon ecological UHPC. *Constr. Build. Mater.* 327, 126921. doi:10.1016/j.conbuildmat.2022.126921

Dong, S. K., Zhuo, Q., Chen, L. L., Wu, F. F., and Xie, L. L. (2023). Reuse of pretreated red mud and phosphogypsum as supplementary cementitious material. *Sustainability* 15 (4), 2856. doi:10.3390/su15042856

Gencel, O., Koksal, F., Erdongmus, E., Ozel, C., Koksal, F., Erdogmus, E., et al. (2012). Properties of concrete paving blocks made with waste marble. *J.Cleaner Prod.* 21, 62–70. doi:10.1016/j.jclepro.2011.08.023

Grabias-Blicharz, E., and Franus, W. (2023). A critical review on mechanochemical processing of fly ash and fly ash-derived materials. *Sci. Total Environ.* 860, 160529. doi:10.1016/j.scitotenv.2022.160529

Guo, R., Xia, H., Yan, Y., and Wang, Z. (2022). Fracture behavior of basalt fiber-reinforced airport pavement concrete at different strain rates. *Materials* 15 (20), 7379. doi:10.3390/ma15207379

He, T. S., Li, Z. B., Zhao, S. Y., Zhao, X. G., and Qu, X. L. (2021). Study on the particle morphology, powder characteristics and hydration activity of blast furnace slag prepared by different grinding methods. *Constr. Build. Mater.* 270, 121445. doi:10.1016/j.conbuildmat.2020.121445

Hlobil, M., Sotiriadis, K., and Hlobilova, A. (2022). Scaling of strength in hardened cement pastes - unveiling the role of microstructural defects and the susceptibility of C-S-H gel to physical/chemical degradation by multiscale modeling. *J. Cem. Concr. Res.* 154, 106714. doi:10.1016/j.cemconres.2022.106714

Hu, Y. R., Zuo, X. B., Li, X. N., and Jiang, D. Q. (2021). Investigation on alkalinity of pore solution and microstructure of hardened cement-slag pastes in purified water. *J. Adv. Concr. Constr.* 12 (6), 507–515. doi:10.12989/acc.2021.12.6.507

Huang, J. S., Li, W. W., Huang, D. S., Wang, L., Chen, E., Wu, C. Y., et al. (2021). Fractal analysis on pore structure and hydration of magnesium oxysulfate cements by first principle, thermodynamic and microstructure-based methods. *Fractal. Fract.* 5 (4), 164. doi:10.3390/fractalfract5040164

Javed, U., Shaikh, F. U. A., and Kumar, P. (2022). Microstructural investigation of lithium slag geopolymer pastes containing silica fume and fly ash as additive chemical modifiers. *Cem. Concr. Compos.* 134, 104736. doi:10.1016/j.cemconcomp.2022.104736

Jian, H., Li, S., and Huanhuan, L. (2016). Testing and analysis on progressive collapse-resistance behavior of RC frame substructures under a side column removal scenario. *J. Perform. Constr. Facil.* 30, 04016022. doi:10.1061/(ASCE)CF.1943-5509.0000873

Li, B. L., Cao, R. L., You, N. Q., Chen, C., and Zhang, Y. M. (2019). Products and properties of steam cured cement mortar containing lithium slag under partial immersion in sulfate solution. *Constr. Build. Mater.* 220, 596–606. doi:10.1016/j.conbuildmat.2019.06.062

Li, J. Z., and Huang, S. W. (2020). Recycling of lithium slag as a green admixture for white reactive powder concrete. *J. Material Cycles Waste Manag.* 22, 1818–1827. doi:10.1007/s10163-020-01069-4

Li, M., Liu, H., Duan, P., Ruan, S. q., Zhang, Z. H., and Wen, G. (2021). The effects of lithium slag on microstructure and mechanical performance of metakaolin-based geopolymers designed by response surface method (RSM). *Constr. Build. Mat.* 299, 123950. doi:10.1016/j.conbuildmat.2021.123950

Li, X., and Yan, P. Y. (2010). Microstructural variation of hardened cement-fly ash pastes leached by soft water. *Sci. China-Technological Sci.* 53, 3033–3038. doi:10.1007/s11431-010-4107-0

Li, Z. N., Shen, A. Q., Yang, X. R., Guo, Y. C., and Liu, Y. W. (2023). A review of steel slag as a substitute for natural aggregate applied to cement concrete. *Road Mater. Pavement Des.* 24 (2), 537–559. doi:10.1080/14680629.2021.2024241

Liu, R. G., Ding, S. D., and Yan, P. Y. (2015). The microstructure of hardened Portland cement-slag complex binder pastes cured under two different curing conditions. *J. Chin. Ceram. Soc.* 43, 610–661. doi:10.14062/j.issn.0454-5648.2015.05.10

Lu, D., Ma, L. P., Zhong, J., Tong, J., Liu, Z. B., Ren, W. C., et al. (2023). Growing nanocrystalline graphene on aggregates for conductive and strong smart cement composites. *ACS Nano* 17, 3587–3597. doi:10.1021/acsnano.2c10141

Luo, Q., Wang, Y. S., Hong, S. X., Xing, F., and Dong, B. Q. (2021). Properties and microstructure of lithium-slag-based geopolymer by one-part mixing method. *Constr. Build. Mater.* 273, 121723. doi:10.1016/j.conbuildmat.2020.121723

Mehdizadeh, H., Shao, X., Mo, K. H., and Ling, T. C. (2022). Enhancement of early age cementitious properties of yellow phosphorus slag via CO_2 aqueous carbonation. *Cem. Concr. Compos.* 133, 104702. doi:10.1016/j.cemconcomp.2022.104702

Peng, Y. X., Tang, S. W., Huang, J. S., Tang, C., Wang, L., and Liu, Y. F. (2022). Fractal analysis on pore structure and modeling of hydration of magnesium phosphate cement paste. *Fractal Fract.* 6 (6), 337. doi:10.3390/fractalfract6060337

Shi, K. B., Wu, F. F., and Bai, X. J. (2020). *Study on the effect of replacing part of cement with lithium slag and fly ash on concrete performance*. Beijing, China: China Water and Power Press.

Singh, M., and Siddique, R. (2014). Strength properties and microstructural properties of concrete containing coal bottom ash as partial replacement of fine aggregate. *Constr. Build. Mater.* 50, 246–256. doi:10.1016/j.conbuildmat.2013.09.026

Snellings, R., Machner, A., Bolte, G., Kamyab, H., Durdzinski, P., Teck, P., et al. (2022). Hydration kinetics of ternary slag-limestone cements: Impact of water to binder ratio and curing temperature. *Cem. Concr. Res.* 151, 106647–106714. doi:10.1016/j.cemconres.2021.106647

Tan, H., Li, M., He, X., Su, Y., Yang, J., and Zhao, H. (2020). Effect of wet grinded lithium slag on compressive strength and hydration of sulphoaluminate cement system. *Constr. Build. Mater.* 267, 120465. doi:10.1016/j.conbuildmat.2020.120465

Topcu, I. B., and Bilir, T. (2010). Effect of bottom ash as fine aggregate on shrinkage cracking of motars. *Aci Mater. J.* 107 (1), 48–56. doi:10.14359/51663465

Turhan, B., Osman, G., and Ilker, B. T. (2015). Properties of mortars with fly ash as fine aggregate. *Constr. Build. Mater.* 93, 782–789. doi:10.1016/j.conbuildmat.2015.05.095

Wang, J., Han, L., Liu, Z., and Wang, D. (2020b). Setting controlling of lithium slag-based geopolymer by activator and sodium tetraborate as a retarder and its effects on mortar properties. *Cem. Concr. Compos.* 110, 103598. doi:10.1016/j.cemconcomp.2020.103598

Wang, L., Huang, Y. J., Zhao, F., Huo, T. T., Chen, E., and Tang, S. W. (2022). Comparison between the influence of finely ground phosphorous slag and fly ash on frost resistance, pore structures and fractal features of hydraulic concrete. *Fractal Fract.* 6 (10), 598. doi:10.3390/fractalfract6100598

Wang, N. N., Sun, X. Y., Zhao, Q., Yang, Y., and Wang, P. (2020a). Leachability and adverse effects of coal fly ash: A review. *J. Hazard. Mater.* 396, 122725. doi:10.1016/j.jhazmat.2020.122725

Wu, F. F., Dong, S. K., Gong, J. W., Chen, L. L., Li, D. S., and Shi, K. B. (2016a). Calculation of concrete with mineral admixture hydration products volume fraction and its influential factors. *Trans. Chin. Soc. Agric. Eng. Trans. CSAE)* 32, 48–54. doi:10.11975/j.issn.1002-6819.2016.03.008

Wu, F. F., Shi, K. B., Dong, S. K., Chen, L. L., Ci, J., Wang, X., et al. (2016b). Influence of admixture and water-cement ratio on hydration products and mechanical properties of cement-based materials. *Trans. Chin. Soc. Agric. Eng. Trans. CSAE)* 32, 119–126. doi:10.11975/j.issn.1002-6819.2016.04.017

Wu, M., Zhang, Y., Liu, G., Wu, Z., Yang, Y., and Sun, W. (2018). Experimental study on the performance of limebased low carbon cementitious materials. *Constr. Build. Mater.* 168, 780–793. doi:10.1016/j.conbuildmat.2018.02.156

Xian, X., and Shao, Y. (2021). Microstructure of cement paste subject to ambient pressure carbonation curing. *Constr. Build. Mater.* 296, 123652. doi:10.1016/j.conbuildmat.2021.123652

Yang, Q., Li, C., Ren, Q., and Jiang, Z. (2021). Properties and microstructure of CO_2 activated binder produced by recycling phosphorous slag. *Constr. Build. Mater.* 282, 122698. doi:10.1016/j.conbuildmat.2021.122698

Yong, C. L., Mo, K. H., and Koting, S. (2022). Phosphorus slag in supplementary cementitious and alkali activated materials: A review on activation methods. *Constr. Build. Mater.* 352, 129028. doi:10.1016/j.conbuildmat.2022.129028

Youm, K. S., Jeong, Y. J., Han, E. S. H., and Yun, T. S. (2014). Experimental investigation on annual changes in mechanical properties of structural concretes with various types of lightweight aggregates. *Constr. Build. Mater.* 73, 442–451. doi:10.1016/j.conbuildmat.2014.09.044

Zhang, H., Wang, L. L., Li, J. J., and Kang, F. (2023). Embedded PZT aggregates for monitoring crack growth and predicting surface crack in reinforced concrete beam. *Constr. Build. Mater.* 364, 129979. doi:10.1016/j.conbuildmat.2022.129979